ACS OMEGA

http://pubs.acs.org/journal/acsodf

Article

Role of the Human Serum Albumin Protein Corona in the Antimicrobial and Photothermal Activity of Metallic Nanoparticles against *Escherichia coli* Bacteria

Alexa Guglielmelli,*[,‖] Patrizia D'Aquila,[‖] Giovanna Palermo,* Marcella Dell'Aglio, Giuseppe Passarino, Giuseppe Strangi, and Dina Bellizzi

Cite This: *ACS Omega* 2023, 8, 31333−31343

Read Online

ACCESS | Metrics & More | Article Recommendations | Supporting Information

ABSTRACT: The emergence of antibiotic-resistant bacteria has become a major public health concern, leading to growing interest in alternative antimicrobial agents. The antibacterial activity of metal nanoparticles (NPs) has been extensively studied, showing that they can effectively inhibit the growth of various bacteria, including both Gram-positive and -negative strains. The presence of a protein corona, formed by the adsorption of proteins onto the NP surface in biological fluids, can significantly affect their toxicity. Understanding the effect of the protein corona on the antimicrobial activity of metal NPs is crucial for their effective use as antimicrobial agents. In this study, the antimicrobial activity of noble metal NPs, such as platinum (Pt), silver (Ag), and gold (Au) with and without the human serum albumin (HSA) protein corona against *Escherichia coli* strains, was investigated. In addition, the plasmonic photothermal effect related to AuNPs, which resulted to be the most biocompatible compared to the other considered metals, was evaluated. The obtained results suggest that the HSA protein corona modulated the antimicrobial activity exerted by the metal NPs against *E. coli* bacteria. These findings may pave the way for the investigation and development of innovative nanoapproaches to face antibiotic resistance emergence.

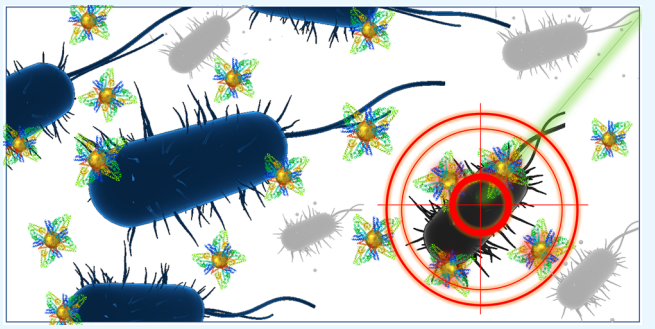

INTRODUCTION

The emergence of bacterial resistance to conventional antibiotics has led to an urgent need for new antimicrobial medicines. Despite many efforts in the development of new antibiotics in the last 50 years, also due to the "innovation gap", the problem of bacterial resistance continues to worsen.[1] Metal nanoparticles (NPs), such as gold (Au), silver (Ag), copper (Cu), palladium (Pd), and platinum (Pt), have been proposed as promising candidates as antimicrobial agents, thanks to their ability to induce death or limit the growth of microorganisms, due to their unique physicochemical properties, including a high surface area-to-volume ratio, high reactivity, and stability. The exact mechanism of the action of metal NPs is not yet fully understood, but it seems to involve various mechanisms, such as oxidative stress, disruption of cell membrane integrity, and DNA damage.[2,3] Despite their promising antibacterial activity, the use of metal NPs also raises concerns regarding their potential toxicity. In fact, to safely use any nanomaterial in bioapplications, it is crucial to ensure their bioactivity and biocompatibility. The NPs' interaction with various biomolecules, within a biological environment, leads to structural and functional modification of both the bio and metal entities. When metal NPs come into contact with biological fluids or living systems, such as blood or cell culture media, proteins and other biomolecules can adsorb onto their surface, forming a protein corona, whose properties depend on the size, shape, and surface properties of the NP.[4−6] The intrinsic function of a protein is strictly related to its unique 3D structure, and therefore, even a small change in the protein structure can significantly affect its function. Depending on the characteristics of the protein corona, it can be classified into two main types: soft and hard protein coronas.[7,8] A soft protein corona is characterized by dynamic and reversible adsorption of proteins onto the NP surface. The proteins in the soft corona are generally weakly bound. In contrast to the soft protein corona, the hard protein corona refers to a more stable and tightly bound layer of proteins on the NP surface. The proteins forming the hard corona have a higher affinity for the NP surface. Understanding the differences between soft and hard protein corona formation

Received: May 29, 2023
Accepted: June 29, 2023
Published: August 18, 2023

is crucial for the design and development of metallic NPs for various biomedical applications. The protein corona not only affects the structure and function of the protein itself but also alters the bioactivity of the coated NP. In some cases, the protein corona may act as a protective barrier around the NPs, reducing their direct interaction with bacteria and consequently diminishing their bactericidal effects. On the other hand, certain proteins in the corona may facilitate the binding and uptake of metal NPs by bacteria, enhancing their antimicrobial activity. The composition and nature of the proteins in the corona depend on various factors, including the surrounding biological environment and the physicochemical properties of the NPs. Understanding the influence of the protein corona on the bactericidal effect of metal NPs is an active area of research to optimize their applications and ensure their safety and efficacy. In this context, several studies have investigated the impact of the protein corona on the bactericidal potential of metal NPs and explored strategies to prevent or enhance its effects. For example, it is well known that silver nanoparticles (AgNPs) are ideal antimicrobial agents due to their effectiveness against a broad spectrum of bacteria and drug-resistant microorganisms.[9] However, the interaction of AgNPs with proteins may alter their inherent bactericidal potential.[10] In particular, it was found that the formation of the bovine serum albumin (BSA) protein corona led to a decrease in the bactericidal potential of the AgNPs against *Escherichia coli* bacteria.[10] In another study, it was demonstrated that BSA could broaden the antibacterial capabilities of non-antibiotic small molecule-capped AuNPs.[1] The authors showed that BSA could enhance the stability and antibacterial activity of AuNPs, suggesting that albumin could be used as a protein corona to improve the therapeutic efficacy of NPs.[1] Similarly, the antibacterial activity of monodisperse (BSA)-conjugated zinc oxide NPs (ZnONPs) was explored.[11] The study demonstrated that BSA could stabilize and enhance the bactericidal potential of ZnONPs, suggesting that protein corona formation could be exploited to improve the antimicrobial activity of NPs. In addition, the presence of a protein corona can impact the immune response to NPs and affect the targeting and delivery of drugs.[12] Overall, these studies highlight the significant influence of protein corona formation in the biological activity of NPs, suggesting strategies for harnessing the protein corona to control the therapeutic efficacy of NPs.

Metal NPs also offer the opportunity to achieve an effective highly targeted photothermal effect, exploiting the conversion of light into heat following the localized surface plasmon resonance (LSPR) process.[13] Due to its proven therapeutic efficacy against bacterial infections and limited collateral effect, photothermal therapy (PTT) has been proposed as a valid alternative treatment against focused infections.[14−17] Therefore, combining a suitable protein corona with the photothermal conversion of metal NPs could represent a promising combined approach to enhance the efficiency of antimicrobial nanosolutions.[18]

In this study, we have considered three highly stable colloidal solutions of spherical Pt, Ag, and Au plasmonic NPs. The NPs were produced by employing pulsed laser ablation in liquid (PLAL) in order to obtain NPs without any kind of contaminants. Then, NPs were incubated with human serum albumin (HSA). The HSA protein corona formation on the three metallic NPs was investigated by means of spectroscopic and morphological analysis. The antibacterial properties of the NPs with and without the HSA protein corona were investigated against the *E. coli* strain. PtNPs and AgNPs showed increasing cytotoxic effects as a function of the used concentrations, while AuNPs proved to be the most biocompatible at all of the concentrations taken into consideration. The presence of an HSA protein corona mitigated the antimicrobial effect of the three metallic NPs. Finally, the photothermal properties of AuNPs were suitably employed to locally increase the temperature in *E. coli* inducing a reduction in cell growth, improved by the presence of the HSA protein corona. The HSA protein corona did not affect the photothermal heating of AuNPs.

This study elucidates the mitigation mechanism of the antibacterial effect performed by the protein corona on different types of metal NPs and suggests that a synergistic use with the photothermal properties of these classes of nanomaterials can provide a valid contribution to the fight against antibiotic resistance. Understanding the dynamic interactions between metal NPs, HSA, and bacteria is essential for evaluating the overall bactericidal effect and optimizing the design and application of NP-based antimicrobial systems.

EXPERIMENTAL SECTION

Materials. Fatty acid-free and globulin-free human serum albumin (type A-3782, purity approximately 99%) was purchased from Sigma-Aldrich (St. Louis).

Synthesis of Platinum, Silver, and Gold Metal Nanoparticles. NPs were produced by PLAL employing a NdYAG laser (Quanta System PILS-GIANT) operating with a 1064 nm laser wavelength, a pulse duration of 6 ns, a fluence of 64 J cm^{-2}, and a laser frequency of 10 Hz. The laser was focused on a target immersed in Milli-Q water using a 5 cm focal lens. The focal plane of the laser beam was chosen inside the target for obtaining a laser crater of (1 ± 0.2) mm. All targets were purchased from Kurt J. Lesker Company (99.999 % pure pellet for Au, 99.99% pure pellet for Ag and Pt). Before the NP production, each target was accurately cleaned first by lapping the surface with an aluminum oxide 150 mesh and then by washing it with soap followed by several rinses with Milli-Q water in a sonicator.[19] The concentration and size of NPs were measured with SPR and DLS, respectively.

Protein Corona Preparation. The three colloidal solutions of metal NPs were incubated with 25 μM HSA for 24 h. The HSA concentration was chosen in order to operate in excess of protein. The obtained NP solutions were centrifuged for 1 h at 20,000*g* to remove the unbound proteins. The supernatant was eliminated and the remaining NP pellet was resuspended in ultrapure water. This procedure was repeated three times to ensure that all unbound proteins were removed.

Characterization of Metal Nanoparticles. *Dynamic Light Scattering.* DLS measurements were performed using a Zetasizer-Nano ZS from Malvern Instruments. The measurements were carried out at 25 °C in backscattering mode and at a fixed detector angle of 173°. Four replicas were acquired for each sample.

UV−vis Spectroscopy. UV−vis absorption spectra were acquired with a UV−vis Spectrophotometer (Cary 5000, Agilent Technologies).

Transmission Electron Microscopy. In order to observe the protein corona, that was formed around the metallic NPs, the samples were first diluted with 1 mL of water and then 2 μL were placed onto a lacey grid and let to dry. The TEM was

https://doi.org/10.1021/acsomega.3c03774
ACS Omega 2023, 8, 31333−31343

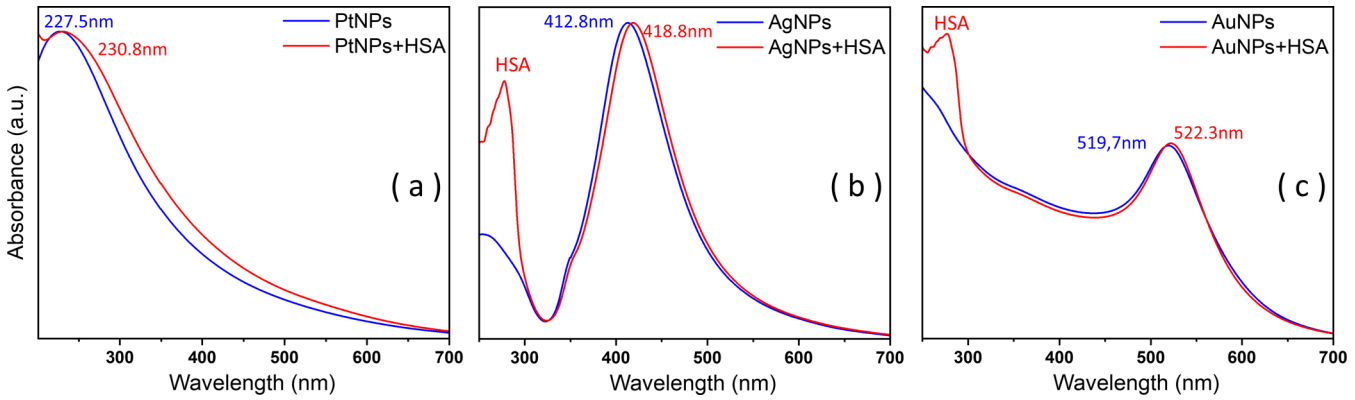

Figure 1. Normalized UV−vis spectra of the bare (blue curves) and with the HSA protein corona (red curves): (a) PtNPs, (b) AgNPs, and (c) AuNPs.

operated at 120 kV. Gadolinium acetate tetrahydrate (10 %w) was added as a contrast agent to label HSA.

Scanning Electron Microscopy. SEM (scanning electron microscopy) images were acquired using a quanta FEG 400 (FEI) in high vacuum mode and an ETD (Everhart−Thornley Detector) sensor type by dehydrating both *E. coli* and *E. coli* + AuNPs and *E. coli* + AuNPs + HSA solutions on glass ITO chips.

Circular Dichroism Spectroscopy. Circular dichroism (CD) spectra were recorded with a Jasco J-1700 spectropolarimeter in a quartz cuvette with a 2 mm path length in the range of 190−260 nm, under constant N_2 supply. The spectra were measured in triplicate with a scan speed of 50 nm/min, a bandwidth of 1.0 nm, a resolution of 0.2 nm, and a PMT voltage of below 600 V. The baseline was subtracted using water as a blank. The raw CD signal (θ) was then converted to mean residue molar ellipticity (θ_{MR}) using the following equation

$$[\theta_{MR}] = \frac{\theta \cdot C \cdot l}{R} \quad (1)$$

where C is the protein concentration, l is the cuvette path length (2.0 mm), and R is the number of amino acid (AA) residues (585 for HSA). The CD spectra were analyzed for secondary structural elements using the software package CD Multivariate SSE.

Bacterial Strain and Growth Conditions. This study was carried out on the *E. coli* strain JM109 (Stratagene, La Jolla, CA) (e14(McrA$^-$) recA1 endA1 gyrA96 thi-1 hsdR17 (r_{K^-} m_{K^+}) supE44 relA1 Δ(lac-proAB) [F' traD36 proAB lacI^{q}ZΔM15]) cultured in Luria-Bertani broth, containing 5 g/L yeast extract, 10 g/L tryptone, and 10 g/L sodium chloride, at 37 °C under agitation. The bacterial strain was kept frozen in stock cultures at −80 °C in cryovials.

Vital Count. Approximately 10^7 cells from an overnight culture were inoculated into a 96-well plate containing 200 μL of serial dilutions of the NPs as well as HSA (2.5−12.5) μM. The tested ranges of concentrations for the three metallic NPs are 0.66−3.3 nM for PtNPs, 0.39−1.95 nM for AgNPs, and 1.28−6.4 nM for AuNPs. Plates were shaken at 300 rpm at 37 °C for 18 h. In all experiments, media with (positive control) and without (negative control) cells and free of NPs were also analyzed to check the microbial growth and sterility, respectively. Turbidity measurement was performed at 600 nm in a spectrophotometer. The vital count was determined by subculturing diluted samples in LB medium, plating by diffusion on LB-agar medium, and incubating at 37 °C overnight. At the end of the incubation, the colonies were counted. The total number of viable cells was determined by multiplying the average number of colonies counted by the adopted dilution factor.

Photothermal Experiments. The thermo-optical experiment was performed with a customized thermo-optical setup with a resonant CW green laser (gem532, Laser Quantum, Stockport, UK) with a wavelength of 532 nm overlapping the plasmonic band of AuNPs to induce the light-triggered localized heating. The sample, contained in a glass tube, was photoexcited from above, with the laser (beam diameter = 8 mm) incident perpendicularly at the center. The spatial temperature distribution and the temperature−time profile were investigated with a high-resolution thermal camera (FLIR A655sc, FLIR System, OR). The software FLIR Research IR Max was used for monitoring and analyzing IR image sequences acquired during laser irradiation. The sample emissivity was set to 0.89 (glass tube), and the camera−sample working distance was 20 cm.

Statistical Analysis. Statistical analyses were performed using SPSS 20.0 statistical software (SPSS Inc., Chicago, IL). One-way analysis of variance (ANOVA) and Student's *t*-test were adopted. The significance level was defined as $p \leq 0.05$.

RESULTS AND DISCUSSION

Spectroscopic and Morphological Analysis of Metal NPs. In this work, both NPs and NP−protein conjugates were employed for the experiments. The chosen NPs were AuNPs, AgNPs, and PtNPs, while HSA was incubated with AuNPs, AgNPs, and PtNPs to obtain nanoparticle protein conjugates. HSA, which has free cysteine residue, shows a high affinity for the surface of the noble metal due to the presence of a single free exterior thiol. It is well known that the interaction between proteins and NPs can be dependent on the NP size.[20−22] The NP curvature can influence the adsorption of protein on the NP surface inducing conformational changes of the protein with respect to the native structure. First, it was observed that the adsorption of the protein on flat macroscopic surfaces can induce more severe conformational variations than those observed on NP surfaces. In the case of NPs with different sizes, this variation can be more intense for larger NPs (low curvature) than that obtained with smaller NPs (high curvature). In addition, the kinetic of adsorption greatly changes with the variation of curvature. Several studies have been already carried out in the literature on the influence of

https://doi.org/10.1021/acsomega.3c03774
ACS Omega 2023, 8, 31333−31343

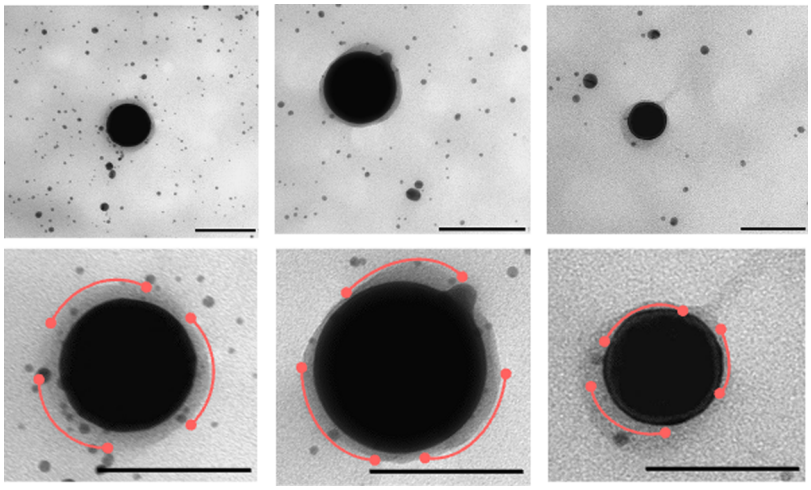

Figure 2. Transmission electron microscopy (TEM) image of PtNPs (first column), AgNPs (second column), and AuNPs (third column) incubated with HSA for 24 h. Red curve lines are added to better highlight the protein corona. The scale bar is 100 nm.

the NP size on the HSA structure.[20,23] In this work, we choose to study the interaction between the NPs at fixed dimensions with the albumin, avoiding the introduction of too many parameters that can vary the interaction between NPs and albumin. Here, the size of NPs was chosen around 10 nm, which has small curvature useful to avoid the interaction between the proteins near one another on the surface. Moreover, it has been demonstrated in ref 24 and in the next paragraph that after the interaction with the spherical AuNPs, albumin undergoes only minor conformational changes in α-helices, which makes this protein suitable for forming stable AuNP−protein conjugates. The employment of different noble metals composing the NPs with similar sizes gives us the opportunity to study the influence of these noble metals on the interactions between the NP−protein conjugates and the bacteria.

A careful optical and morphological characterization of the three spherical metal NP solutions, as synthesized and with the presence of HSA, was performed. The absorption spectra of the three colloidal solutions, of platinum (PtNPs), silver (AgNPs), and gold (AuNPs), in a water-based solution, are reported in Figure 1a−c. From the spectra of the bare NPs (blue curves), it is possible to see the typical plasmon peak, for PtNPs, AgNPs, and AuNPs centered at λ_{LSPR} = (227.5 ± 0.3) nm, λ_{LSPR} = (412.8 ± 0.3) nm, and λ_{LSPR} = (519.7 ± 0.3) nm, respectively.

The LSPR peaks of the three NPs underwent a red shift after the interaction with HSA (red curves), equal to 3.3 nm for PtNPs, 6 nm for AgNPs, and 2.6 nm for AuNPs. Such a red shift is caused by the change in the refractive index surrounding the metal NPs, as previously reported in the literature;[25] the red shift represents clear evidence of the presence of a protein coating, disposed of like a protein corona on the NP surface.[25] In the AgNPs and AuNPs spectra, after the HSA adsorption (red curves, Figure 1), the HSA absorption peak at around 278 nm arising from aromatic amino acid residues is also evident.[26] In the PtNPs + HSA absorption spectrum, the HSA peak overlaps the plasmonic band, so it is not possible to distinguish it. From the plasmon peak shift, it is possible to approximately derive the HSA corona thickness using the following formula[23,27]

$$\frac{\Delta\lambda}{\lambda_0} = 0,18e^{(-\frac{S}{D})/0,22} \quad (2)$$

where $\Delta\lambda/\lambda_0$ is the fractional plasmon shift, S is the distance between the NP surface and the protein, D is the NP diameter, and 0.22 is the decay constant for the universal trend of plot $\Delta\lambda/\lambda_0$ versus S/D.[28] Taking into account an averaged diameter of 10 nm (below the values from DLS measurements are reported) and using eq 2, the corona thickness turns out to be about 5.75 nm for PtNPs, 5.54 nm for AgNPs, and 7.88 nm for AuNPs. Equation 2, known as the ruler equation, provides information about the interparticle separation of NPs considering the absorption spectral shift, and it has already been used in other works to obtain an approximative estimation of the thickness of the absorbed protein layer on the NPs' surface.[23,27,29] The difference in the thickness obtained is in accordance with other studies, showing that the formation of the protein corona depends on the composition of the NPs (core material) and its size.[30] In addition, it was proved that the number of protein binding sites on the NP surface depends strictly on the NP and protein sizes.[31] It is worth emphasizing that the shift in the LSPR band of NPs is not followed by any peak broadening or noticeably higher baseline, indicating that the change in the LSPR band's position is mostly caused by HSA binding on the NP surface rather than NP aggregation.[32] The absence of aggregation is also demonstrated by the absence of a color change in the colloidal solutions before and after the addition of the HSA (see Figure S1 in the Supporting Information). To confirm the LSPR results of the NP−protein corona formation, DLS measurements were performed on the bare NPs and on the NP + HSA conjugates, whose preparation was reported in the section Materials and Methods. As already told, the number of proteins needed to bind the whole surface of the NPs depends on both sizes of NP and protein. The averaged hydrodynamic diameters, measured from the DLS NP size distributions, were (10 ± 2) nm, (9 ± 3) nm, and (10 ± 2) nm for PtNPs, AgNPs, and AuNPs, respectively. The NP + HSA conjugate hydrodynamic diameters were (30.5 ± 3) nm, (18.0 ± 3) nm, and (21.6 ± 3) nm for PtNP + HSA, AgNP + HSA, and AuNP + HSA, respectively. These results, within the error of measurement, confirm the HSA thickness calculated with the red shift of the LSPR peaks. Taking into account that DLS average

https://doi.org/10.1021/acsomega.3c03774
ACS Omega 2023, 8, 31333−31343

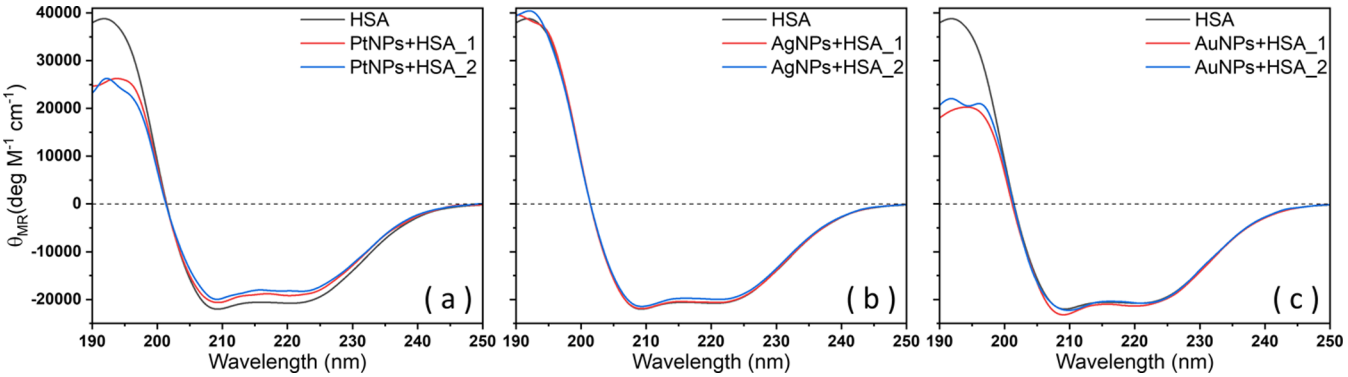

Figure 3. Circular dichroism spectra, reported in mean residue molar ellipticity θ_{MR}, of HSA and (a) PtNPs, (b) AgNPs, and (c) AuNPs incubated with HSA for 15 min (1) and 24 h (2).

diameters of both NP (d_{NP}) and NP+protein conjugate (d_{NP+HSA}) were measured, the thicknesses ($(d_{NP+HSA} - d_{NP})/2$) of the protein coronas were 9.9 nm (PtNPs + HSA), 4.5 nm (AgNPs + HSA), and 5.3 nm (AuNPs + HSA). By considering the HSA gyration radius of 2.6 nm[33] and considering in first approximation the HSA shape as a sphere in physical contact with the NP surface, we can see how the found values are similar to the diameters of the HSA, except the one obtained for the PtNP+HSA conjugate. Here, we cannot exclude the possibility of the formation of more than one corona.

The morphological analysis, conducted with transmission electron microscopy (TEM), on the NP solutions highlighted the absence of aggregates, before and after the formation of the protein corona. The HSA corona presence is confirmed by the TEM analysis reported in Figure 2, where the presence of a halo around the NP surface occurred after the interaction with the protein. Clear visualization of the protein corona by TEM analysis was only possible around the NPs characterized by a diameter greater than 50 nm, even if this diameter is not representative of the average size of NPs. This last was around 10 nm for all NPs considered here, as measured with LSPR and DLS techniques and visible from the TEM images themselves. However, this visualization is not indicative that the protein corona is not present even on the smallest NPs. The plasmon shift (Figure 1) and the hydrodynamic diameters of NP + HSA conjugates reported in the previous sections confirm the adsorption of HSA on the surface of small NPs, too.

We further monitored the interaction between metallic nanoparticles and HSA using circular dichroism (CD) spectroscopy. The CD spectrum of the free HSA in water (Figure 3, black curve) is characterized by the strong positive peak at 191 nm, due to the $\pi \rightarrow \pi^*$ transition, and two weaker but broader negative peaks at 209 and 222 nm, due to the $\pi \rightarrow \pi^*$ and $n \rightarrow \pi^*$ transitions, respectively, typical of proteins that mainly present an α-helical structure.[34] In particular, by analyzing the CD spectra with JASCO secondary structure estimation software, with an optimized ad hoc calibration model, we calculated 61.9% of the α-helix, 13.3% of the β-sheet, 8.8% of turn, and 16.1% of other structures (see Table 1). Then, to monitor the HSA secondary structure in the presence of the three metallic nanoparticles, the CD spectra of PtNPs, AgNPs, and AuNPs incubated with HSA for 15 min and 24 h were recorded and analyzed. In the presence of NPs, the intensity of these bands decreased to different extents, depending on the metal NPs, without any shift of the peaks, and an isodichroic point was observed at 201.4 nm. The

Table 1. Calculated Fractions of Different Secondary Structures in % for HSA and PtNPs, AgNPs, and AuNPs Incubated with HSA for 15 min (1) and 24 h (2)[a]

	α-helix (%)	β-helix (%)	turn (%)	others (%)
HSA	61.9	13.3	8.8	16.1
PtNPs + HSA_1	56.1	14.1	10.7	19.2
PtNPs + HSA_2	35.0	24.5	11.6	28.8
AgNPs + HSA_1	71.9	10.1	6.9	11.2
AgNPs + HSA_2	44.2	24.5	8.4	23.0
AuNPs + HSA_1	50.7	7.8	15.0	26.3
AuNPs + HSA_2	19.7	41.4	14.0	24.8

[a]The fitting percentage uncertainty is 2%.

isodichroic point indicates the presence of two-state dichroic models (bound and unbound states) during the interaction with NPs.[8] Figure 3a–c shows a decrease of CD signals at 191, 208, and 222 nm, highlighting the fact that HSA + NPs interactions take place and influence the HSA secondary structural elements. The drop denotes the decrease in the α-helical component content of the protein. CD spectra of NPs were also recorded in the absence of HSA, showing no CD signal, as the spherical nanoparticles are inherently achiral. Therefore, one may consider that the presence of nanoparticles in the protein + NPs conjugates should not affect the CD signal of the protein, assuming that the protein conformation is retained after conjugation. So, this result clearly proved that the protein is interacting with the nanoparticles causing a change in its secondary structure. In detail, the calculated fractions α-helix secondary structure of HSA after 15 min of incubation with the nanoparticles changed from 61.9% (±2%) to 56.1% (±2%) with PtNPs, to 71.9% (±2%) with AgNPs, and to 50.7% (±2%) with AuNPs.

In addition, CD spectroscopy could be used to distinguish the formation of a soft corona from a hard protein corona by looking at the preservation of the HSA secondary structure after the incubation with nanoparticles. In particular, if the secondary structure is preserved, showing small differences with respect to the native state, it is assumed that the HSA formed a soft corona around NPs; otherwise, if the secondary structure is partially lost, then the protein corona can be defined as a hard corona.[7,35] The CD spectrum observed for PtNPs + HSA and AuNPs + HSA after 15 min showed a partial unfolding of α-helices, from 61.9% (±2%) to 56.1% (±2%) and to 50.7% (±2%), respectively (Figure 3a,b), suggesting a rapid hard interaction, while the absence of significant changes in the CD spectra of AgNPs+HSA after 15

https://doi.org/10.1021/acsomega.3c03774
ACS Omega 2023, 8, 31333−31343

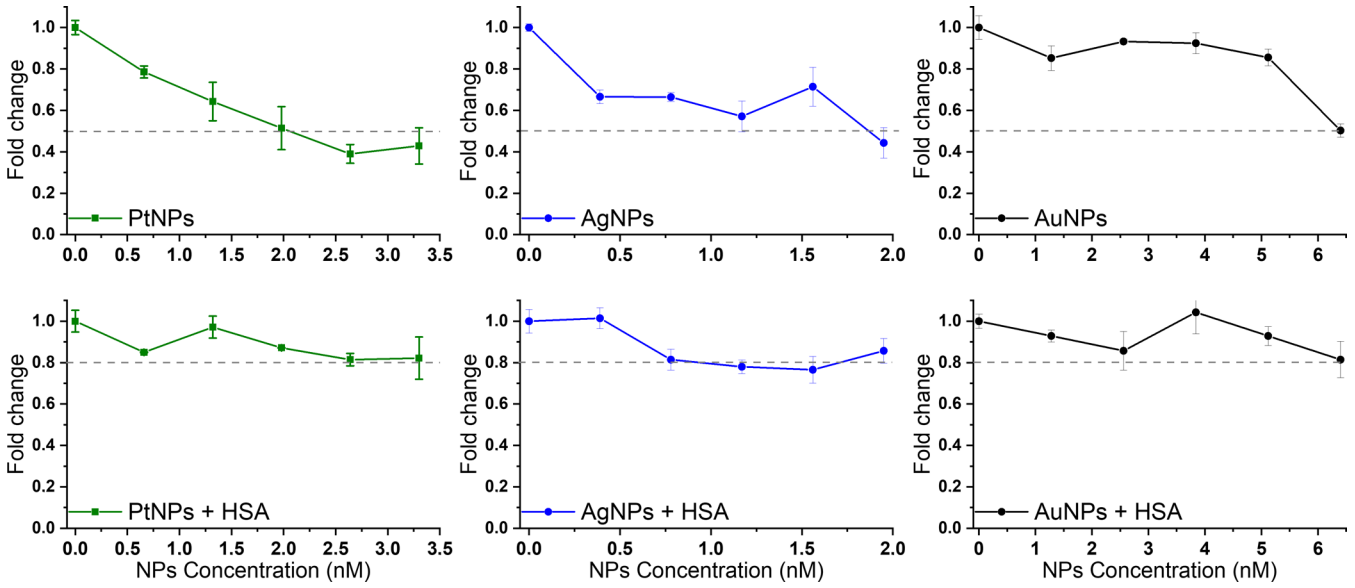

Figure 4. Antibacterial activity of the three metal nanoparticles, as synthesized (upper row) and with HSA corona (lower row) against *E. coli*, as a function of increasing NP concentration. The values represent the mean of three independent triplicate experiments with standard error.

min of incubation suggests the presence of soft interaction (Figure 3c). After 24 h of incubation, the fractions of α-helices drastically decrease for all three metal NPs. These conformational changes can be attributed to the direct adsorption of HSA onto the NP surface and the free energy minimization within this newly formed complex.[7] These results show that variations in HSA CD signals after the addition of Au/Ag/PtNPs can be assigned to the local conformational alterations in HSA owing to the interaction. However, the shape and location of the peak indicate that the HSA fundamental structure as a bio-macromolecular model is unaffected.[36] The summary of the secondary structure content of all of the samples is reported in Table 1. In addition, CD spectra were collected at three different incubation times of 6, 12, and 24 h to monitor the stability of the protein corona (see Figure S3 in the Supporting Information).

Antibacterial Activity of Metallic NPs on *E. coli*. The growth inhibition activity of the three metallic solutions was tested on *E. coli* in the Luria-Bertani (LB) medium at different concentrations of the NPs. Figure 4, upper row, shows the growth curve of *E. coli* suspended in contact with different NP concentrations for 24 h, normalized to the control value without NPs. The culture plates were analyzed after the incubation of *E. coli* in the incubator with a constant temperature of 37 °C for 24 h with NPs, before counting the number of colonies. The tested range of concentrations for the three metallic NPs was (i) (0.66−3.3) nM for PtNPs, (ii) (0.39−1.95) nM for AgNPs, and (iii) (1.28−6.4) nM for AuNPs.

The choice to consider different concentrations of the three metallic solutions was dictated by the well-known and different antibacterial properties of the three considered metals.[37,38] In addition, we observed that with the PLAL technique, solutions of the three considered metals characterized by higher concentrations result to be unstable, with consequent precipitation of the metals after few days.

The growth inhibition curve of *E. coli* in the presence of PtNPs showed a gradual decrease with the increase of the NP concentration, reaching a growth reduction of 62% with a concentration of 2.6 nM.

The bacteria growth inhibition effect of AgNPs showed a similar trend, inducing a reduction of 56% of vitality for a concentration of 1.95 nM. AgNPs resulted in superior bacterial growth inhibition with smaller concentrations of NPs, as expected from the literature.[38] The bacteriostatic effect induced by AuNPs revealed a completely different trend. AuNPs were almost completely biocompatible up to concentrations of 5.12 nM, while at the highest concentration of 6.4 nM, they induced a 50% decrease in bacterial growth.

These results illustrate that higher concentrations of metallic NPs are more efficient in inhibiting *E. coli* growth, indicating that the antibacterial efficacy is concentration dependent and also related to the material used.

From Figure 4, upper row, the bacterial colonies left after 24 h of NP incubation at the maximum concentration, with respect to the nontreated colonies, can be observed.

Before testing the NPs with the HSA corona, control experiments to avoid any possible cytotoxic effect due to the mere presence of the protein were carried out, showing the absence of inhibition for all of the tested concentrations of HSA (2.5−12.5 μM) as reported in Figure S2in the Supporting Information.

To investigate the role of the protein corona around the three metallic NPs on *E. coli* growth, the same experiments with the same concentrations used for NPs without HSA were performed. As shown in Figure 4, lower row, the presence of an HSA corona significantly decreased the bacterial inhibition effect with respect to the one obtained with bare NPs, for all of the metal NPs used. The growth inhibition induced in this case never exceeded 20%, as evidenced by the dashed gray line drawn on the three curves in Figure 4, lower row. Taken together, these results suggest that the formation of an HSA corona on the NP surface protects *E. coli* from the antibacterial activity, creating a biocompatible coating around the metals. This result is in accordance with a study[10] that showed the loss of the bactericidal potential of AgNPs due to protein corona formation. In addition, another study affirmed that the

https://doi.org/10.1021/acsomega.3c03774
ACS Omega 2023, 8, 31333−31343

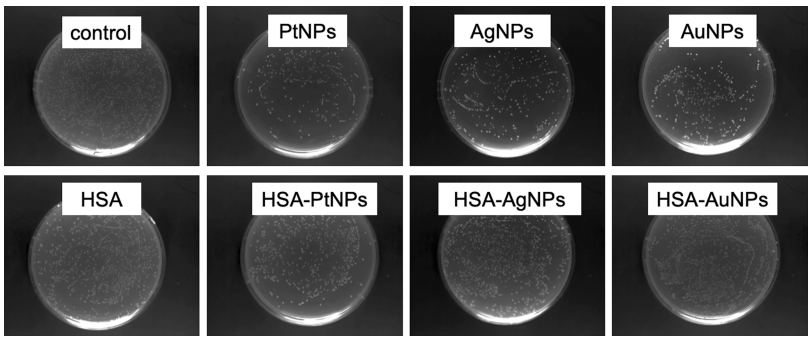

Figure 5. Photographs of colonies of *E. coli* incubated on agar plates obtained from cultivated suspensions with different metallic NP solutions (at a higher concentration), with (lower row) and without (upper row) the HSA protein corona.

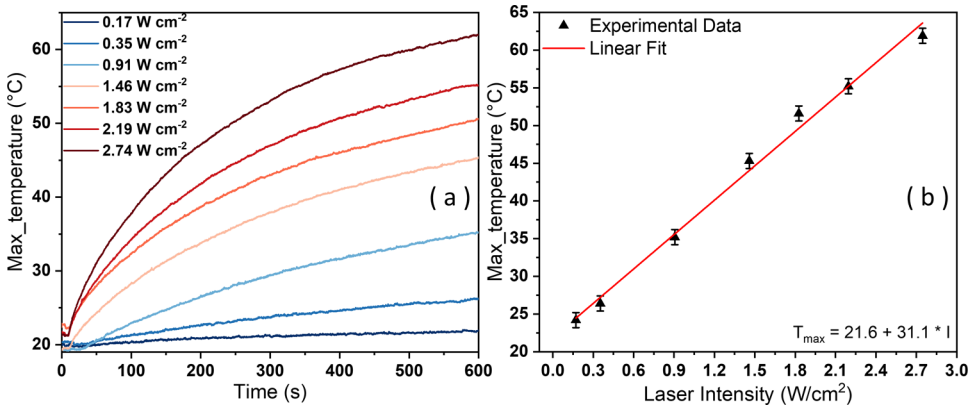

Figure 6. Photothermal characterization of the gold nanoparticles. (a) Time−temperature dependence of gold nanoparticles dispersed in water under pump beam illumination. (b) Linear fit of the temperature variation versus the intensity of the pump beam. The coefficient R^2 = 0.99 indicates the goodness of fit.

interaction of AgNPs with serum albumin in the blood can alter their antibacterial effects.[39] Different possible explanations about the mitigation of the cytotoxicity played by the HSA corona were given, such as the biodegradation of Ag ions, the decline of the agglomeration rate, and the reduction of reactive oxygen species.[40] Figure 5, lower row, further confirms the biocompatible capping effect of HSA, as evidenced by the presence of a greater number of bacterial colonies than those found with the same concentrations of NPs alone (Figure 5, upper row).

Time-dependent studies were also performed to assess the growth inhibition of E. *coli* in the presence of AuNPs (6.4 nM) with and without the HSA corona at different incubation times (6, 12, 24 h) to observe any temporal changes in the inhibitory effect and obtain information on the kinetics of bacterial growth inhibition (see Figure S5 in the Supporting Information).

Scanning electron microscopy (SEM) analysis was carried out to examine the morphology and interaction of the metallic NPs with *E. coli* in the presence and absence of the HSA corona. This analysis provides visual evidence of the binding and localization of AuNPs on and near the bacterial cell membrane, in both cases (see Figure S4 in the Supporting Information).

To broaden the scope of the study and assess the generalizability of the results, some preliminary cell viability tests, with NPs and NPs+HSA for 24 h incubation, were performed on two pathogenic bacteria strains. In particular, we have chosen *Enterococcus faecalis* (*E. Faecalis*), which is a Gram-positive bacteria, and *Chromobacterium Violaceum* (*C. Violaceum*), which is a Gram-negative bacteria (data not shown). For all bacterial strains, and the concentrations of NPs tested, the presence of the protein corona seems to exert a protective effect, decreasing and in some cases completely canceling the antimicrobial efficacy of the metal NPs. These preliminary results, although promising, need to be replicated and will be the subject of future studies.

Photothermal Experiments. AuNPs were tested to investigate their photothermal conversion efficiency when exposed to a 532 nm wavelength laser source in resonance with their LSPR peak. The colloidal solution was irradiated for 10 min with different laser intensities from 0.17 to 2.74 W cm^{-2}. The maximum temperature reached as a function of time was monitored by using a photothermal camera. The time−temperature curves are reported in Figure 6a.

As theoretically expected,[13,41] the photothermal response increased with increasing irradiation intensity (I), and it is well described by a linear trend (see Figure 6b). With higher laser intensity, after 10 min of irradiation, the maximum temperature (T_{max}) reached in the AuNPs sample was 62 °C (see Figure 6a). These temperature values are sufficient for irreversibly injuring biological samples, (including viral particles, bacteria, tumoral cells),[42] leading to a dramatic activation of cell death above 48 °C and instantaneous and irreversible protein denaturation above 60 °C.[43] The photothermal efficiency of AuNPs is directly related to the absorption cross sections σ_{abs} and inversely related to the sum of the absorption and scattering cross sections (σ_{abs} + σ_{sca}). For small spherical AuNPs ($d \approx 10-20$ nm), the σ_{sca} is negligible; thus, the photothermal efficiency is comparable to

https://doi.org/10.1021/acsomega.3c03774
ACS Omega 2023, 8, 31333−31343

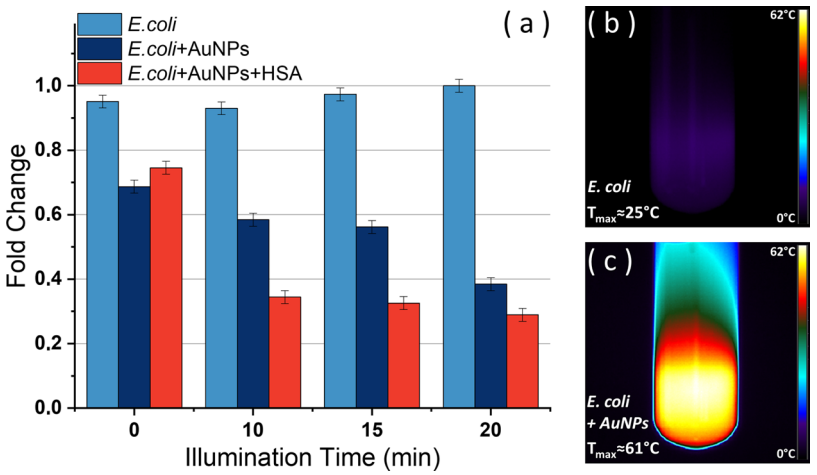

Figure 7. (a) Results of the viability experiments carried out with and without AuNPs and AuNPs+HSA at three different illumination times, along with representative infrared thermographic images of (b) *E. coli* and (c) *E. coli* + NPs samples after 20 min of laser irradiation. The values represent the mean of three independent triplicate experiments with standard error.

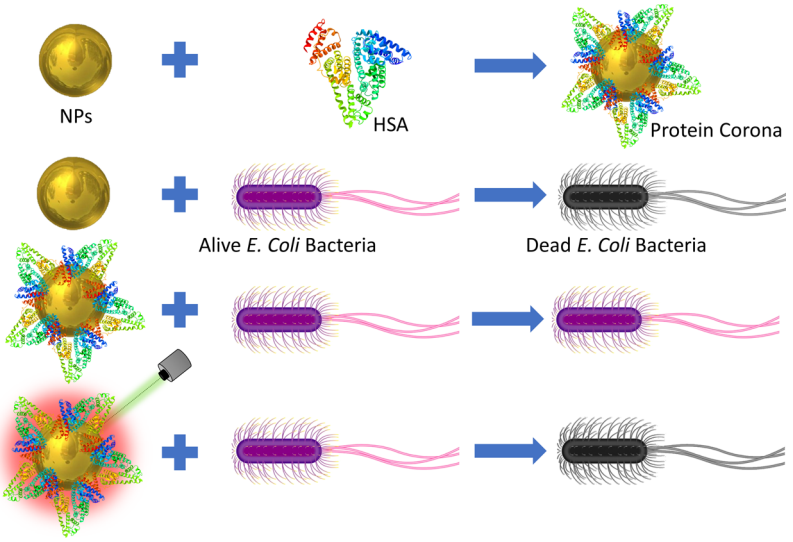

Figure 8. Schematic representation of the interaction between HSA and AuNPs, and the effect on *E. coli* bacteria with and without 532 nm laser irradiation.

1.[44] Encouraged by the excellent photothermal performance of the AuNPs, it was decided to carry out photothermal therapy experiments by irradiating the *E. coli* bacteria containing the AuNPs (5.12 nM) at different irradiation times (10, 15, 20 min). The results of the photothermally induced antibacterial effect of AuNPs containing the *E. coli* sample, as a function of the illumination time, are shown in Figure 7a. The *E. coli* sample incubated with AuNPs reached 52.5, 57.9, and 60.8 °C after 10, 15, and 20 min of laser irradiation, respectively. Figure 7c provides a representative thermographic image of the sample *E. coli* + AuNPs after 20 min of laser irradiation, showing a uniform distribution of the phototriggered heating. These temperatures induced a reduction of the cell viability of 39, 42, and 60% respectively, showing a trend of viability reduction depending on the radiation dose. To investigate the effect of the HSA corona on thermally induced inhibitory capabilities, the same photothermal experiment was performed with AuNPs + HSA at the same concentration. The maximum temperatures reached for the *E. coli* samples with AuNPs+HSA were 50.6, 57.1, and 60.2 °C after 10, 15, and 20 min of laser irradiation respectively, so comparable with those obtained in the absence of the protein corona. The photothermal heating of AuNPs + HSA was not affected by protein corona formation, as observed in other photothermal applications.[45]

Although the temperatures reached are almost identical to those obtained in the absence of HSA, the effects induced on bacterial growth are significantly different (see Figure 7a). The results obtained in the presence of the HSA corona demonstrated an enhancement of the antibacterial effects induced by the photoexcited AuNPs. The obtained reduction of the cell viability was 64% for 10 min of laser irradiation, 66% for 15 min of laser irradiation, and 70% for 20 min of laser irradiation. It is worth noting that the control experiments conducted by irradiating *E. coli* without the addition of AuNPs did not show any temperature change (see Figure 7b) and, consequently, no reduction in cell viability, highlighting that the inhibition effect is induced by the presence of plasmonic nanoheaters and not by the visible laser. The absence of photoinduced temperature increase in the *E. coli* sample after 20 min of irradiation can be clearly deduced from the infrared

https://doi.org/10.1021/acsomega.3c03774
ACS Omega 2023, 8, 31333−31343

thermograph shown in Figure 7b. The results obtained, in the case of AuNPs with the protein corona, can be explained by taking into account that HSA guarantees the anchoring of the protein−NP bioconjugate to bacteria, facilitating their absorption and the consequent rupture of the membrane due to the high localized increase of the photoinduced temperature. These findings (schematically represented in Figure 8) can be attributed to the altered NP surface characteristics known to enforce cell adhesion and cellular uptake.[46]

CONCLUSIONS

In summary, we have evaluated the antimicrobial effect of Pt/Ag/AuNPs obtained with the PLAL technique against *E. coli* bacteria in the presence or absence of the HSA protein corona. HSA is one of the most abundant proteins found in human blood plasma and can readily adsorb onto the surface of NPs. Importantly, for the concentration of HSA and metal NPs considered in this study, HSA mitigates the metal NP toxicity against *E. coli* bacteria. Among the three metals tested, as expected, albeit considered a higher concentration than the other two metals, Au proved to be the most tolerated by microorganisms, without inducing significant effects on bacterial growth. AuNPs with and without the HSA corona demonstrated a high photothermal conversion efficiency and a significant photoinduced effect improved by the presence of HSA. Our study suggests that HSA represents a biocompatible coating for metal NPs; NPs + HSA corona-mediated photothermal therapy is a convenient strategy for bacteria treatment and enhances the potential of NP antimicrobial applications.

ASSOCIATED CONTENT

Supporting Information

The Supporting Information is available free of charge at https://pubs.acs.org/doi/10.1021/acsomega.3c03774.

> Photo of the colloidal NP solutions before and after HSA addition; survival histogram of *E. coli* bacteria after the treatment with different concentrations of HSA between 2.5 and 12.5 μM; CD spectra of HSA, and HSA + PtNPs, + AgNPs, and + AuNPs at three different incubation times, 6, 12, and 24 h; SEM micrograph of *E. coli*, *E. coli* + AuNPs, *E. coli* + AuNPs + HSA, and *E. coli* + AuNPs + HSA after photoactivation, deposited on an ITO chip; and time-dependent studies to assess the growth inhibition of *E. coli* in the presence of AuNPs at the maximum concentration, with and without the HSA corona, at different incubation times (6, 12, and 24 h) (PDF)

AUTHOR INFORMATION

Corresponding Authors

Alexa Guglielmelli − *Department of Physics, NLHT-Lab, University of Calabria and CNR-NANOTEC, Institute of Nanotechnology, 87036 Rende, Italy;* orcid.org/0000-0002-0792-659X; Email: alexa.guglielmelli@unical.it

Giovanna Palermo − *Department of Physics, NLHT-Lab, University of Calabria and CNR-NANOTEC, Institute of Nanotechnology, 87036 Rende, Italy;* orcid.org/0000-0001-5649-735X; Email: giovanna.palermo@unical.it

Authors

Patrizia D'Aquila − *Department of Biology, Ecology and Earth Sciences, University of Calabria, 87036 Rende, Italy*

Marcella Dell'Aglio − *CNR-IFN, Institute for Photonics and Nanotechnologies, c/o Physics Department, University of Bari, 70126 Bari, Italy;* orcid.org/0000-0002-9639-6489

Giuseppe Passarino − *Department of Biology, Ecology and Earth Sciences, University of Calabria, 87036 Rende, Italy*

Giuseppe Strangi − *Department of Physics, NLHT-Lab, University of Calabria and CNR-NANOTEC, Institute of Nanotechnology, 87036 Rende, Italy; Department of Physics, Case Western Reserve University, Cleveland, Ohio 44106, United States*

Dina Bellizzi − *Department of Biology, Ecology and Earth Sciences, University of Calabria, 87036 Rende, Italy*

Complete contact information is available at: https://pubs.acs.org/10.1021/acsomega.3c03774

Author Contributions

‖A.G. and P.D. contributed equally to this work.

Notes

The authors declare no competing financial interest.

ACKNOWLEDGMENTS

A.G., G.P., and G.S. acknowledge financial support from the "NLHT - Nanoscience Laboratory for Human Technologies" (POR Calabria FESR-FSE 14/20) and thank Dr. G. Desiderio (CNR-NANOTEC, Institute of Nanotechnology, Rende, Italy) for the SEM analysis. M.D. would like to thank Prof. G. Palazzo and Prof. A. De Giacomo of the Chemistry Department (Univ. of Bari-Italy) for the DLS measurements and for the discussion on the NP−protein conjugate behavior, respectively.

REFERENCES

(1) Sun, Z.; Zheng, W.; Zhu, G.; Lian, J.; Wang, J.; Hui, P.; He, S.; Chen, W.; Jiang, X. Albumin broadens the antibacterial capabilities of nonantibiotic small molecule-capped gold nanoparticles. *ACS Appl. Mater. Interfaces* **2019**, *11*, 45381−45389.

(2) Slavin, Y. N.; Asnis, J.; Hńfeli, U. O.; Bach, H. Metal nanoparticles: understanding the mechanisms behind antibacterial activity. *J. Nanobiotechnol.* **2017**, *15*, No. 65.

(3) Shaikh, S.; Nazam, N.; Rizvi, S. M. D.; Ahmad, K.; Baig, M. H.; Lee, E. J.; Choi, I. Mechanistic insights into the antimicrobial actions of metallic nanoparticles and their implications for multidrug resistance. *Int. J. Mol. Sci.* **2019**, *20*, 2468.

(4) Fahmy, S. A.; Preis, E.; Bakowsky, U.; Azzazy, H. M. E.-S. Platinum nanoparticles: green synthesis and biomedical applications. *Molecules* **2020**, *25*, 4981.

(5) Durán, N.; Silveira, C. P.; Durán, M.; Martinez, D. S. T. Silver nanoparticle protein corona and toxicity: a mini-review. *J. Nanobiotechnol.* **2015**, *13*, No. 55.

(6) Yinhua, D.; Foroughi, M. M.; Aramesh-Boroujeni, Z.; Jahani, S.; Peydayesh, M.; Borhani, F.; Khatami, M.; Rohani, M.; Dusek, M.; Eigner, V. The synthesis, characterization, DNA/BSA/HSA interactions, molecular modeling, antibacterial properties, and in vitro cytotoxic activities of novel parent and niosome nano-encapsulated Ho (III) complexes. *RSC Adv.* **2020**, *10*, 22891−22908.

(7) Kihara, S.; Van Der Heijden, N. J.; Seal, C. K.; Mata, J. P.; Whitten, A. E.; Koper, I.; McGillivray, D. J. Soft and hard interactions between polystyrene nanoplastics and human serum albumin protein corona. *Bioconjugate Chem.* **2019**, *30*, 1067−1076.

(8) Liu, W.; Rose, J.; Plantevin, S.; Auffan, M.; Bottero, J.-Y.; Vidaud, C. Protein corona formation for nanomaterials and proteins of a similar size: hard or soft corona? *Nanoscale* **2013**, *5*, 1658−1668.

(9) Lara, H. H.; Ayala-Núnez, N. V.; Ixtepan Turrent, L. d. C.; Rodríguez Padilla, C. Bactericidal effect of silver nanoparticles against multidrug-resistant bacteria. *World J. Microbiol. Biotechnol.* **2010**, *26*, 615−621.
(10) Ban, D. K.; Paul, S. Protein corona over silver nanoparticles triggers conformational change of proteins and drop in bactericidal potential of nanoparticles: Polyethylene glycol capping as preventive strategy. *Colloids Surf., B* **2016**, *146*, 577−584.
(11) Wu, D.; Chen, Z.; Cai, K.; Zhuo, D.; Chen, J.; Jiang, B. Investigation into the antibacterial activity of monodisperse BSA-conjugated zinc oxide nanoparticles. *Curr. Appl. Phys.* **2014**, *14*, 1470−1475.
(12) Corbo, C.; Molinaro, R.; Parodi, A.; Toledano Furman, N. E.; Salvatore, F.; Tasciotti, E. The impact of nanoparticle protein corona on cytotoxicity, immunotoxicity and target drug delivery. *Nanomedicine* **2016**, *11*, 81−100.
(13) Baffou, G.; Quidant, R. Thermo-plasmonics: using metallic nanostructures as nano-sources of heat. *Laser Photonics Rev.* **2013**, *7*, 171−187.
(14) He, D.; Yang, T.; Qian, W.; Qi, C.; Mao, L.; Yu, X.; Zhu, H.; Luo, G.; Deng, J. Combined photothermal and antibiotic therapy for bacterial infection via acidity-sensitive nanocarriers with enhanced antimicrobial performance. *Appl. Mater. Today* **2018**, *12*, 415−429.
(15) Bermúdez-Jiménez, C.; Romney, M. G.; Roa-Flores, S. A.; Martínez-Castañón, G.; Bach, H. Hydrogel-embedded gold nanorods activated by plasmonic photothermy with potent antimicrobial activity. *Nanomedicine* **2019**, *22*, No. 102093.
(16) Younis, M. R.; An, R. B.; Yin, Y.-C.; Wang, S.; Ye, D.; Xia, X.-H. Plasmonic nanohybrid with high photothermal conversion efficiency for simultaneously effective antibacterial/anticancer photothermal therapy. *ACS Appl. Bio Mater.* **2019**, *2*, 3942−3953.
(17) Chen, Y.; Gao, Y.; Chen, Y.; Liu, L.; Mo, A.; Peng, Q. Nanomaterials-based photothermal therapy and its potentials in antibacterial treatment. *J. Controlled Release* **2020**, *328*, 251−262.
(18) Huang, J.; Zhou, J.; Zhuang, J.; Gao, H.; Huang, D.; Wang, L.; Wu, W.; Li, Q.; Yang, D.-P.; Han, M.-Y. Strong near-infrared absorbing and biocompatible CuS nanoparticles for rapid and efficient photothermal ablation of gram-positive and-negative bacteria. *ACS Appl. Mater. Interfaces* **2017**, *9*, 36606−36614.
(19) Dell'Aglio, M.; Mangini, V.; Valenza, G.; De Pascale, O.; De Stradis, A.; Natile, G.; Arnesano, F.; De Giacomo, A. Silver and gold nanoparticles produced by pulsed laser ablation in liquid to investigate their interaction with ubiquitin. *Appl. Surf. Sci.* **2016**, *374*, 297−304.
(20) Piella, J.; Bastús, N. G.; Puntes, V. Size-dependent protein-nanoparticle interactions in citrate-stabilized gold nanoparticles: the emergence of the protein corona. *Bioconjugate Chem.* **2017**, *28*, 88−97.
(21) Liu, J.; Peng, Q. Protein-gold nanoparticle interactions and their possible impact on biomedical applications. *Acta biomaterialia* **2017**, *55*, 13−27.
(22) Mahmoudi, M.; Lynch, I.; Ejtehadi, M. R.; Monopoli, M. P.; Bombelli, F. B.; Laurent, S. Protein- nanoparticle interactions: opportunities and challenges. *Chem. Rev.* **2011**, *111*, 5610−5637.
(23) Lacerda, S. H. D. P.; Park, J. J.; Meuse, C.; Pristinski, D.; Becker, M. L.; Karim, A.; Douglas, J. F. Interaction of gold nanoparticles with common human blood proteins. *ACS Nano* **2010**, *4*, 365−379.
(24) Tsai, D.-H.; DelRio, F. W.; Keene, A. M.; Tyner, K. M.; MacCuspie, R. I.; Cho, T. J.; Zachariah, M. R.; Hackley, V. A. Adsorption and conformation of serum albumin protein on gold nanoparticles investigated using dimensional measurements and in situ spectroscopic methods. *Langmuir* **2011**, *27*, 2464−2477.
(25) Hooshmand, N.; Thoutam, A.; Anikovskiy, M.; Labouta, H. I.; El-Sayed, M. Localized surface plasmon resonance as a tool to study protein corona formation on nanoparticles. *J. Phys. Chem. C* **2021**, *125*, 24765−24776.
(26) Guglielmelli, A.; Rizzuti, B.; Guzzi, R. Stereoselective and domain-specific effects of ibuprofen on the thermal stability of human serum albumin. *Eur. J. Pharm. Sci.* **2018**, *112*, 122−131.
(27) Ashkarran, A. A.; Ghavami, M.; Aghaverdi, H.; Stroeve, P.; Mahmoudi, M. Bacterial effects and protein corona evaluations: crucial ignored factors in the prediction of bio-efficacy of various forms of silver nanoparticles. *Chem. Res. Toxicol.* **2012**, *25*, 1231−1242.
(28) Jain, P. K.; Huang, W.; El-Sayed, M. A. On the universal scaling behavior of the distance decay of plasmon coupling in metal nanoparticle pairs: a plasmon ruler equation. *Nano Lett.* **2007**, *7*, 2080−2088.
(29) Mehrdel, B.; Othman, N.; Aziz, A. A.; Khaniabadi, P. M.; Jameel, M. S.; Dheyab, M. A.; Amiri, I. Identifying metal nanoparticle size effect on sensing common human plasma protein by counting the sensitivity of optical absorption spectra damping. *Plasmonics* **2020**, *15*, 123−133.
(30) del Pilar Chantada-Vázquez, M.; López, A. C.; Bravo, S. B.; Vázquez-Estévez, S.; Acea-Nebril, B.; Núñez, C. Proteomic analysis of the bio-corona formed on the surface of (Au, Ag, Pt)-nanoparticles in human serum. *Colloids Surf., B* **2019**, *177*, 141−148.
(31) Dell'Aglio, M.; Salajková, Z.; Mallardi, A.; Sportelli, M. C.; Kaiser, J.; Cioffi, N.; De Giacomo, A. Sensing nanoparticle-protein corona using nanoparticle enhanced Laser Induced Breakdown Spectroscopy signal enhancement. *Talanta* **2021**, *235*, 122741.
(32) Selva Sharma, A.; Ilanchelian, M. Comprehensive multi-spectroscopic analysis on the interaction and corona formation of human serum albumin with gold/silver alloy nanoparticles. *J. Phys. Chem. B* **2015**, *119*, 9461−9476.
(33) Olivieril, J. R.; Craievich, A. F. The subdomain structure of human serum albumin in solution under different pH conditions studied by small angle X-ray scattering. *Eur. Biophys. J.* **1995**, *24*, 77−84.
(34) Li, S.; Peng, Z.; Leblanc, R. M. Method to determine protein concentration in the protein-nanoparticle conjugates aqueous solution using circular dichroism spectroscopy. *Anal. Chem.* **2015**, *87*, 6455−6459.
(35) Kihara, S.; Ghosh, S.; McDougall, D. R.; Whitten, A. E.; Mata, J. P.; Köper, I.; McGillivray, D. J. Structure of soft and hard protein corona around polystyrene nanoplastics—Particle size and protein types. *Biointerphases* **2020**, *15*, No. 051002.
(36) Panahi, R.; Jafarirad, S.; Samadi, A.; Barzegar, A. Synthesis, Characterization and Fluorescence Properties of Novel Porous Fe/ZnO Nano-Hybrid Assemblies by Using Berberis Thunbergii Extract. *J. Fluoresc.* **2021**, *31*, 1191−1202.
(37) Yadav, N.; Jaiswal, A. K.; Dey, K. K.; Yadav, V. B.; Nath, G.; Srivastava, A. K.; Yadav, R. R. Trimetallic Au/Pt/Ag based nanofluid for enhanced antibacterial response. *Mater. Chem. Phys.* **2018**, *218*, 10−17.
(38) R, N.; Nishanthi, R.; S, M.; Malathi, S.; S, J. P.; Palani, P. Green synthesis and characterization of bioinspired silver, gold and platinum nanoparticles and evaluation of their synergistic antibacterial activity after combining with different classes of antibiotics. *Mater. Sci. Eng. C* **2019**, *96*, 693−707.
(39) Gnanadhas, D. P.; Ben Thomas, M.; Thomas, R.; Raichur, A. M.; Chakravortty, D. Interaction of silver nanoparticles with serum proteins affects their antimicrobial activity in vivo. *Antimicrob. Agents Chemother.* **2013**, *57*, 4945−4955.
(40) He, J.; Wei, Q.; Wang, S.; Hua, S.; Zhou, M. Bioinspired protein corona strategy enhanced biocompatibility of Ag-Hybrid hollow Au nanoshells for surface-enhanced Raman scattering imaging and on-demand activation tumor-phototherapy. *Biomaterials* **2021**, *271*, No. 120734.
(41) Pezzi, L.; Palermo, G.; Veltri, A.; Cataldi, U.; Bürgi, T.; Ritacco, T.; Giocondo, M.; Umeton, C.; De Luca, A. Photo-thermal study of a layer of randomly distributed gold nanoparticles: From nano-localization to macro-scale effects. *J. Phys. D: Appl. Phys.* **2017**, *50*, No. 435302.
(42) Huang, X.; Jain, P. K.; El-Sayed, I. H.; El-Sayed, M. A. Plasmonic photothermal therapy (PPTT) using gold nanoparticles. *Lasers Med. Sci.* **2008**, *23*, 217−228.

https://doi.org/10.1021/acsomega.3c03774
ACS Omega 2023, 8, 31333−31343

(43) Annesi, F.; Pane, A.; Losso, M. A.; Guglielmelli, A.; Lucente, F.; Petronella, F.; Placido, T.; Comparelli, R.; Guzzo, M. G.; Curri, M. L.; et al. Thermo-plasmonic killing of *Escherichia coli* TG1 bacteria. *Materials* **2019**, *12*, 1530.
(44) De Sio, L.; Cataldi, U.; Guglielmelli, A.; Bürgi, T.; Tabiryan, N.; Bunning, T. J. Dynamic optical properties of gold nanoparticles/cholesteric liquid crystal arrays. *MRS Commun.* **2018**, *8*, 550−555.
(45) Yeo, E. L. L.; Joshua, U.; Cheah, J.; Neo, D. J. H.; Goh, W. I.; Kanchanawong, P.; Soo, K. C.; Thong, P. S. P.; Kah, J. C. Y. Exploiting the protein corona around gold nanorods for low-dose combined photothermal and photodynamic therapy. *J. Mater. Chem. B* **2017**, *5*, 254−268.
(46) Langiu, M.; Dadparvar, M.; Kreuter, J.; Ruonala, M. O. Human serum albumin-based nanoparticle-mediated in vitro gene delivery. *PLoS One* **2014**, *9*, No. e107603.

https://doi.org/10.1021/acsomega.3c03774
ACS Omega 2023, 8, 31333−31343